ELSEVIER

Cement & Concrete Composites 26 (2004) 531–540

Cement & Concrete Composites

www.elsevier.com/locate/cemconcomp

Assessing residual stress development and stress relaxation in restrained concrete ring specimens

Akhter B. Hossain [a], Jason Weiss [b,*]

[a] School of Civil Engineering, Purdue University, West Lafayette, IN 47907, USA
[b] School of Civil Engineering, Purdue University, 1284 Civil Engineering Building, West Lafayette, IN, 47907-1284, USA

Abstract

Recently, the American Association of State Highway and Transportation Officials implemented a provisional standard that uses the 'ring test' to help quantify a materials' propensity for cracking. While this test may provide qualitative information that enables different mixtures to be compared, it does not provide quantitative information to describe how close a specimen is to failure. This paper will describe how the ring test may be used to provide quantitative information about stress development that may be used to assess the potential for cracking in concrete. An analytical stress formulation is presented to compute the actual residual stress level in the concrete using only the measured strain from the steel ring. The theoretical elastic stress is computed using the free shrinkage, ring deformation, and elastic modulus of the concrete. A comparison of the residual and theoretical elastic stress levels provides information about the extent of stress relaxation in a material. Continuously monitoring the strain that develops in the steel ring from the time of casting enables the effects of autogenous shrinkage to be determined as well as the effects of drying shrinkage.

Keywords: Concrete; Cracking; Creep; Early-age; Relaxation; Ring test; Shrinkage

1. Introduction

Portland cement based materials change volume (i.e., shrink or expand) as a result of temperature and moisture variation. If prevented, these volumetric changes can result in the development of residual tensile stresses that may be sufficient to cause cracking. The problem of early-age cracking is receiving significant attention due to the increase in cracking that has been observed in many 'high-performance' concretes [1,2]. Several test methods have been developed to assess the cracking potential of concrete mixtures, a review of which is provided in literature [1,3,4]. Several studies utilize linear specimen geometries due to the advantage of straightforward data interpretation [5–9]. These experiments use either 'passive-restraint' from a test frame to limit length change (i.e., apply restraint) in the concrete [5,10,11] or 'active-restraint' which uses either a hydraulic or electrical actuator to apply a force to counteract the length change due to shrinkage [5–8]. While these 'active-restraint' systems can provide complete restraint along with accurate stress and stiffness history, cost may limit their use in common quality control testing and large-scale parametric evaluations. The passive restraint tests are typically designed to be either very rigid (thereby permitting only negligible movement) or flexible enough to allow strain development in the steel to be measured (thereby providing information on the state of stress in the concrete). Recently it has been shown that movements may occur at the end grips that would have the possibility of further reducing the stress level in a passive restraint test [12].

Due to its simplicity and versatility, the 'ring test' has become commonly used over the last two decades to assess the potential for shrinkage cracking [3,13–17]. The ring test consists of a concrete annulus that is cast around a hollow steel cylinder. As the concrete dries, shrinkage is prevented by the steel ring resulting in the development of tensile stresses in concrete. The ring specimen geometry is frequently preferred for quality control testing and material evaluation since the difficulties associated with providing adequate end restraint are removed. The simple geometry allows the specimen to be fabricated easily while the low cost of the system enables several tests to be conducted concurrently over long periods of time.

* Corresponding author. Tel.: +1-765-494-2215; fax: +1-765-496-1364.
E-mail address: wjweiss@ecn.purdue.edu (J. Weiss).

0958-9465/$ - see front matter © 2003 Elsevier Ltd. All rights reserved.
doi:10.1016/S0958-9465(03)00069-6

The American Association of State Highway and Transportation Officials (AASHTO) developed a provisional standard [18] that recommends a ring with a 300 mm (12 in.) inner diameter, a 75 mm (3 in.) concrete wall thickness, a 150 mm (6 in.) height, and a 12 mm (1/2 in.) steel wall thickness. The standard also includes the use of strain gages which are placed at mid-height on the inner circumference of the steel ring. Strain is monitored over time and abrupt changes in the steel strain are used to signal the age of cracking [3,19]. While the current AASHTO ring test is a step forward in that it provides a systematic test that can be used to compare the age of cracking or crack width that develops in different mixtures, it is limited with respect to providing information about the residual stresses that develop. The current AASHTO approach does not provide direct information on how close a mixture may be to cracking, especially in cases where cracking does not occur. This paper builds on the idea that strain information can be used to quantify the ring test [17,20].

This paper proposes an approach by which the 'ring test' can be utilized to obtain additional information (with minimal additional effort) thereby making the ring test more informative. In this paper the boundary conditions of the ring are modified to enable the stress field to be computed directly thereby permitting comparison between strength and residual stress development. The formulation of equations needed to perform the stress analysis is provided for use with either hand calculations or on a simple spreadsheet thereby further enabling its use for QC/QA testing.

2. Experimental program

This paper describes a technique that utilizes the information from the restrained ring test to obtain useful information, such as stress development in cementitious systems. To illustrate this approach, two series of tests were conducted using mortar. The mortars were made with type I cement, water to cement ratios (w/c) of 0.3 and 0.5 respectively, and a sand volume of 50%. High-range water reducing admixture was added to 0.3 w/c mortar at 3.0% by weight of cement. After mixing, the mortar was placed in the forms, rodded, finished with a steel trowel, placed under a plastic sheet to prevent moisture loss, and maintained at 21 °C for 24 h. The specimens were demolded at an age of 24 h and placed in a 21 °C, 50% RH environment for the remainder of the experiment.

2.1. Specimen geometry

Several different ring specimens were prepared. All of the concrete in the rings had an inner diameter of 300 mm (12 in.) and an outer diameter of 450 mm (18 in.). Several different wall thicknesses of the steel ring were studied including: 3.1 mm (1/8 in.), 9.5 mm (3/8 in.), and 19.0 mm (3/4 in.). Each steel ring used in this study had four strain gages attached at the mid-height of the inner surface of the steel ring. The strain gages were connected to a data acquisition system in a half-bridge configuration for continuous monitoring. Strain data was acquired at 10 min. intervals using the data acquisition system shown in Fig. 1.

The ring tests performed in this study were similar to the AASHTO ring with two exceptions as illustrated in Fig. 2. First the circumference of the concrete ring was sealed immediately after demolding (24 h) using two layers of aluminum tape. To improve the bond between the tape and mortar a thin film of acetate was used during casting to cover the inner surface of the disposable cardboard outer form. This provided a smooth surface on the mortar [21]. By permitting drying from only the top and bottom surface of the ring, moisture is lost along a single plane thereby simplifying modeling and providing uniform moisture loss through the radial dimension of the specimen. The difference between these experiments and the AASHTO method was that the height of the specimen was reduced to 75 mm (3 in.). This was done to increase the shrinkage rate and to

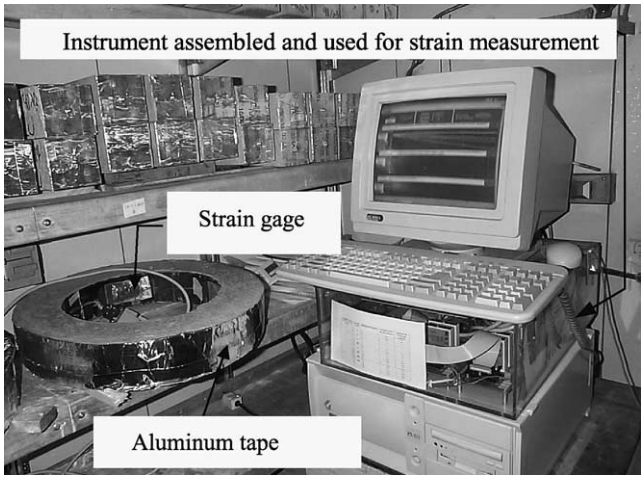

Fig. 1. Illustration of the instrumented restrained ring test.

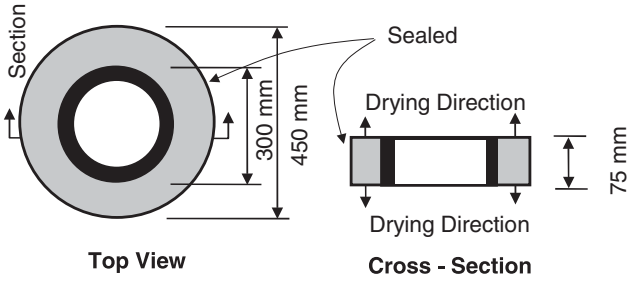

Fig. 2. Restrained ring specimen geometry.

enable a direct comparison to results of test prisms with dimensions that are similar to those used in ASTM C-157 testing [22], 75 mm (3 in.) square cross-section with a 250 mm (10 in.) gage length. The ASTM C-157 test specimens were modified in this study by sealing the two sides and ends of the free shrinkage specimen with aluminum tape, thereby providing identical drying conditions to the concrete in the ring. This implies that the measured free shrinkage from the prism can be compared directly to the ring specimen without the need for any geometric corrections. Autogenous shrinkage was measured between the time of final set and 24 h using an approach that was similar that advocated by the Technical Committee of the Japanese Concrete Institute [23].

In addition to the restrained ring specimens, cylindrical specimens were cast to determine the splitting tensile strength, static elastic modulus, and compressional wave velocity at various ages. The cylinders used for splitting tensile stress determination had a length that was equal to the ring height (75 mm, 3 in.) with a 100 mm (4 in.) diameter, however the remainder of the testing procedure was consistent with that specified by ASTM-C-496 [22]. The elastic modulus was determined according to ASTM-C-469 [22] using cylinders with 200 mm (8 in.) length and 100 mm (4 in.) diameter. In addition the velocity (V_d) of the compressional wave was measured in the concrete cylinders according to ASTM-C-597 [22,24].

2.2. Ring test experimental results

Fig. 3 provides a graphical representation of the average strain data obtained from the ring using the data acquisition system. It can be noticed that the thinner steel rings demonstrate a much higher strain level than the thicker rings. A higher rate of strain development was observed for the lower w/c mixture. For example, at and age of 5 days the 9.5 mm (3/8 in.) ring with 0.3 w/c mortar experiences 128 microstrain whereas the same ring with 0.5 w/c mortar only experiences 74 microstrain. In addition, it can be seen that an abrupt change of strain was observed in several instances which coincided with the age a visible crack was observed. In plain mortars (i.e. non-fiber reinforced), this abrupt change in strain is typically observed to drop to approximately zero strain. It can be seen that strain is measured as early as 3–4 h in the 0.3 w/c mixture as shown in the inset of Fig. 3. This is similar in scale to the times of initial and final set as determined using ASTM-C-403 (pin penetration) [22] for the same mixtures (2.25 and 3.0 h for the 0.3 w/c mixture and 4.0 and 5.25 h for the 0.5 w/c mixture respectively [25]).

2.3. Material property development

Fig. 4 shows the experimental results obtained from shrinkage tests that were performed to describe these materials. Since these experimental results correspond to measured properties at specific times, regression functions were developed to provide a method that could represent the time-dependent material properties at other ages. Free shrinkage strain measurements (ε_{SH}) are represented using Eq. (1).

$$\varepsilon(t)_{SH} = C_1(t - t_0)^{C_2} + C_3\sqrt{t - t_d} \quad (1)$$

In this equation C_1, C_2, and C_3 represent material constants, t is the age of the specimen, t_0 represents the age of the specimen at setting ('time-zero' [26]), and t_d represents the age of the specimen when drying is initiated (i.e., 1 day for this paper). The form of Eq. (1) is based on the approximation that total shrinkage is the sum of an autogenous component (first term) and a drying component (second term). The shape of the second term is based on the observations of Acker (as reported by RILEM TC-69 [27]) who related the initial shape of the drying shrinkage curve to the square root of drying time. Eq. (1) inherently assumes that drying and autogenous shrinkages are independent, which simplifies data

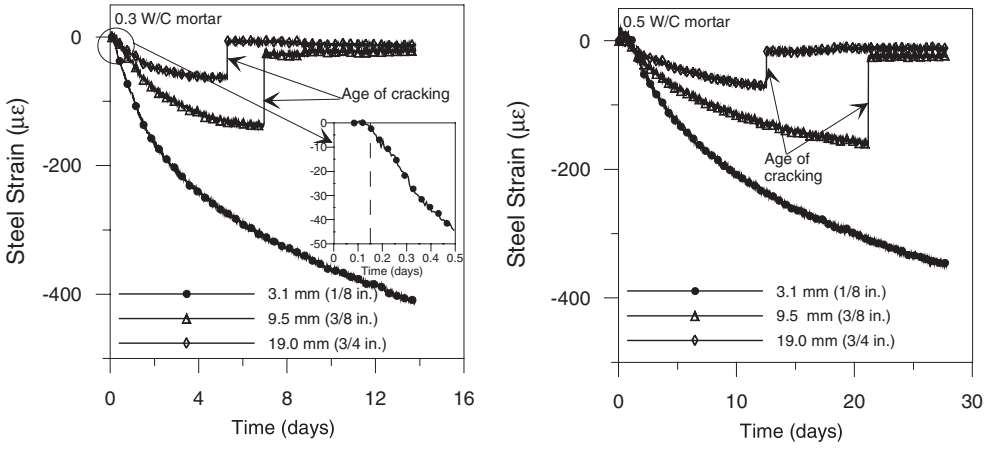

Fig. 3. Average strain in the steel ring.

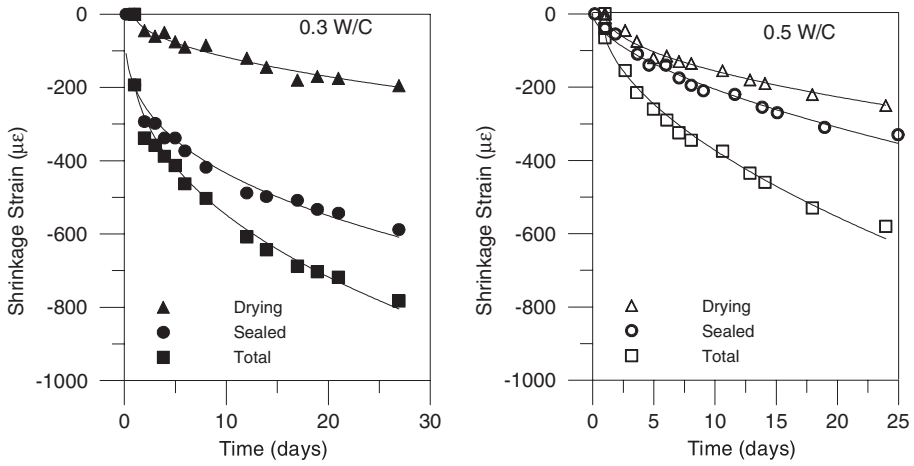

Fig. 4. Regression fits for various shrinkage components.

analysis, though it should be noted that this is not absolutely true. To obtain the material constants C_1 and C_2 shown in Eq. (1) (which correspond with autogenous shrinkage), the shrinkage measured in sealed specimens ($\varepsilon_{\text{Sealed}}$) was fit using Eq. (2).

$$\varepsilon(t)_{\text{Sealed}} = C_1(t - t_0)^{C_2} \tag{2}$$

It should be noted that t_0 is taken as the time of final set. After obtaining values for C_1 and C_2 from the sealed specimen, these values were used in Eq. (1) and the total shrinkage was fit to obtain C_3. Once C_3 is known, the drying component of shrinkage ($\varepsilon_{\text{Drying}}$) (i.e., the difference between the total shrinkage and autogenous shrinkage) can be represented by Eq. (3).

$$\varepsilon(t)_{\text{Drying}} = C_3\sqrt{t - t_{\text{d}}} \tag{3}$$

In addition to determining the development of free shrinkage, expressions were fit to assess the elastic modulus and split-tensile strength as shown in Fig. 5. An approach was taken that is similar to that described by Carino [24] in which the maximum static elastic modulus for a mixture (E_∞) was determined from the intercept of a modulus versus inverse of time graph. At this time it should be noted that previous research [28] illustrated the need for sufficient early-age data to obtain a realistic value for the rate constant, C_4. To obtain sufficient experimental results using a limited number of specimens the dynamic elastic modulus, E_{d}, was determined at frequent intervals using non-destructive testing. Fig. 5 shows a comparison of the ratio of the static and dynamic moduli over time ($E_{\text{S}}/E_{\text{S}\infty}$ and $E_{\text{d}}/E_{\text{d}\infty}$ respectively). It can be seen that the general trend is similar between the two test methods, therefore it appears reasonable to use the ratio of the squared pulse velocities (it can be shown that this is equivalent to the ratio of dynamic moduli) can be used to determine the rate constant C_4. It should be noted however that E_∞ is based on the long-term measurement of the static elastic modulus since the values of the dynamic modulus are typically slightly higher.

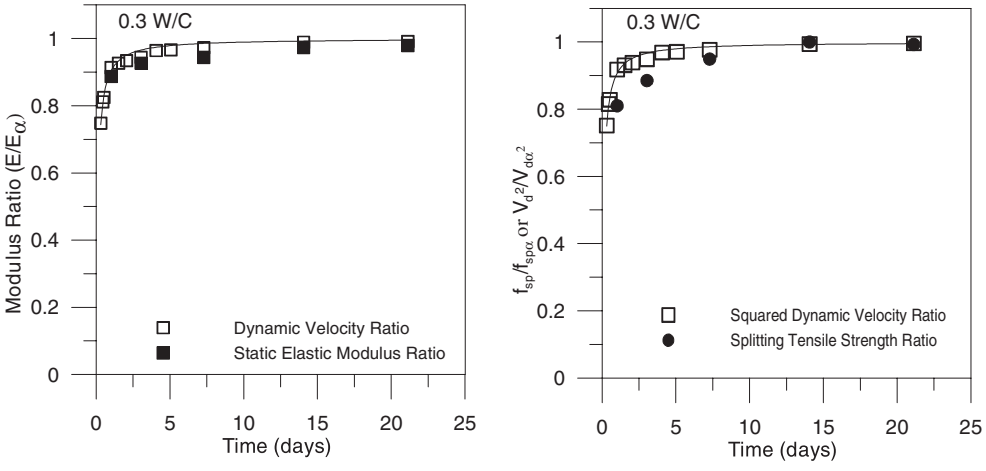

Fig. 5. Regression fits for age-dependent elastic modulus and splitting tensile strength.

Table 1
Regression coefficients

Mixture	C_1	C_2	C_3	C_4	E_∞ (GPa)	$f_{sp\infty}$ (Mpa)
$W/C = 0.3$	−198.70	0.34	−39.20	9.57	30.75	5.29
$W/C = 0.5$	−52.83	0.59	−52.01	2.45	21.37	4.73

$$E(t) = E_\alpha \frac{C_4(t - t_0)}{1 + C_4(t - t_0)} \tag{4}$$

Similarly, the rate constant for split tensile stress can be shown to have a similar gain to that of the squared dynamic velocity ratio ($V_d^2/V_{d\infty}^2$). As a result the rate constant C_4 can be used to describe the rate of splitting tensile strength gain as well.

$$f_{sp}(t) = f_{sp\alpha} \frac{C_4(t - t_0)}{1 + C_4(t - t_0)}$$

The values of regression coefficients C_1 to C_4, E_∞, and $f_{sp\infty}$ shown in Table 1 for the mortars described in this paper.

3. Quantitative analysis of the ring test

To provide a more quantitative analysis of the ring test this paper will employ two stress formulations. The first formulation describes the theoretical elastic stress that develops due to shrinkage if creep (or relaxation) is not considered. The second formulation describes how the actual residual stress that develops in the ring can be calculated directly. Comparison of the actual stress development with the time-dependent strength provides a method for quantifying the risk of cracking while comparison of the theoretical elastic stress and actual stress provides information about the relaxation experienced by the material.

3.1. Determination of the theoretical elastic stress

Previous investigations [16] assumed the stiffness of the steel ring to be high enough that the outer radius of the steel did not deform under loading in an effort to simplify calculations. While appropriate for the solid steel rings used in that investigation, the rings used in this study are much less rigid and consequently the steel can be expected to deform under the loading from the concrete. This section will describe how the compression of the steel ring is used to compute the theoretical elastic stress that would develop in the mortar if no creep occurred.

Fig. 6 provides a conceptual overview of the 'shrink-fit' approach that is chosen to determine the elastic response of the concrete. It can be assumed that initially the steel and concrete rings are in contact with one another (i.e., the outer radius of the steel (R_{OS}) meeting the inner radius of the concrete (R_{IC}) (Fig. 6a)). To solve for the theoretical elastic stress that develops due to shrinkage, consider temporarily removing the restraining effect of the steel thereby permitting the concrete to shrink freely (Fig. 6b). This drying or autogenous shrinkage causes the concrete ring to want to shrink resulting in the inner radius of the concrete ring becoming shorter by an amount ΔU_{SH} which can be calculated directly using Eq. (5):

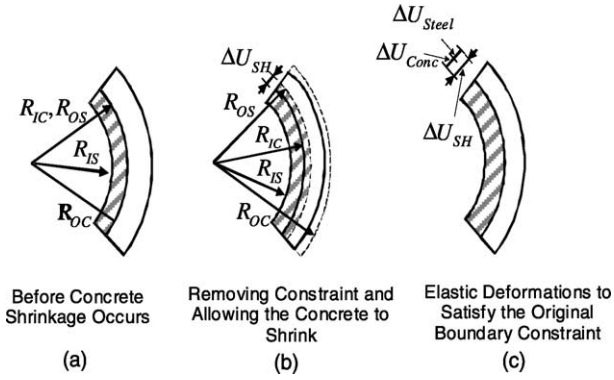

Fig. 6. Geometry of the ring to determine the elastic response: (a) initial condition, (b) releasing restraint, and (c) final geometry satisfying boundary conditions.

$$\Delta U_{SH} = R_{IC} \cdot \Delta\varepsilon_{SH} \tag{5}$$

where $\Delta\varepsilon_{SH}$ is the incremental free shrinkage (negative values correspond to shrinkage) from Eq. (1) and R_{IC} is the inner radius of the concrete ring. At this time it should also be remembered that aluminum tape applied to the outer circumference of the concrete permits uniform shrinkage throughout the radial direction.

To account for the mismatch between the new radius of the concrete ($R_{IC} + \Delta U_{SH}$) and the original outer radius of the steel (R_{IS}), a 'shrink-fit' approach is used (Fig. 6c). A pressurizing force, p_{elas}, can be thought to be applied to the interface between the steel and the concrete. This pressuring force will act to compress the steel ring and expand the concrete ring until displacement compatibility is achieved (i.e., the outer radius of the steel equals the new inner radius of the concrete). The displacement at the outer surface of the steel ring under an external pressure can be calculated using Eq. (6) while the equation that describes the displacement of the inner surface of the concrete ring is provided in Eq. (7).

$$U_S|_{R_{OS}} = -\Delta p_{elas} \frac{R_{OS}^2\left[(1 + \nu_S)R_{IS}^2 + (1 - \nu_S)R_{OS}^2\right]}{E_S R_{OS}(R_{OS}^2 - R_{IS}^2)} \tag{6}$$

$$U_C|_{R_{IC}} = \frac{\Delta p_{elas}}{E_C} \cdot \frac{R_{IC}^2\left[(1 + \nu_C)R_{OC}^2 + (1 - \nu_C)R_{IC}^2\right]}{R_{IC}(R_{OC}^2 - R_{IC}^2)} \tag{7}$$

In these equations R_{IS} and R_{OS} are the inner and outer radius of the steel ring respectively, R_{IC} and R_{OC} are the inner and outer radius of the concrete ring respectively,

v_S and E_S are the Poisson's ratio and elastic modulus of the steel respectively, and v_c and E_c are the Poisson's ratio and elastic modulus of the concrete respectively. It should be noted that R_{IC} is equivalent to R_{OS}.

The condition for displacement compatibility after the necessary elastic pressure is applied is shown in Eq. (8).

$$U_S|_{R_{OS}} - U_C|_{R_{IC}} = \Delta U_{SH} \tag{8}$$

By setting R_{IC} is equal to R_{OS}, Eqs. (5)–(7) can be substituted into (8) and simplified to yield Eq. (9):

$$\Delta p_{elas} = -\frac{\Delta\varepsilon_{SH} E_C}{\frac{E_C}{E_S} C_{1R} + C_{2R}} \tag{9}$$

where C_{1R}, and C_{2R} can be assumed to be constant for a given geometry as shown in Eqs. (10a) and (10b) if Poisson's ratio for concrete is assumed not to vary as a function of time ($v_c = 0.18$).

$$C_{1R} = \frac{\left[(1+v_S)R_{IS}^2 + (1-v_S)R_{OS}^2\right]}{(R_{OS}^2 - R_{IS}^2)} \tag{10a}$$

$$C_{2R} = \frac{\left[(1-v_C)R_{OS}^2 + (1+v_C)R_{OC}^2\right]}{(R_{OC}^2 - R_{OS}^2)} \tag{10b}$$

It should be noted that Eq. (9) provides a solution for the interface pressure in which $\Delta\varepsilon_{SH}$ and E_c are the only variables that will vary as a function of time (Eqs. (1) and (4) respectively).

Once the interface pressure is determined from Eq. (9), the tensile stress (circumferential) in the ring at any point along the radial direction in the concrete ring can be computed using the elastic stress solution for a pressurized cylinder shown in Eq. (11) [29]:

$$\Delta\sigma_\theta(r) = \Delta p_{elas} \frac{R_{OS}^2}{R_{OC}^2 - R_{OS}^2}\left(1 + \frac{R_{OC}^2}{r^2}\right) \tag{11}$$

The maximum tensile stress always occurs at the interface between the concrete and steel (i.e., $r = R_{OS}$). This enables Eq. (11) to be rewritten in terms of the maximum tensile stress as shown in Eq. (12).

$$\Delta\sigma_{\theta-max} = \Delta p_{elas} C_{3R} \tag{12}$$

where C_{3R} is a geometry constant given as

$$C_{3R} = \frac{R_{OS}^2 + R_{OC}^2}{R_{OC}^2 - R_{OS}^2} \tag{12b}$$

It can be shown that C_{3R} is a constant that depends on the ratio of the concrete radii, R_{OC}/R_{IC}. Substituting Eq. (9) into Eq. (12) provides an expression for the maximum incremental tensile stress as shown in (13):

$$\Delta\sigma_{Elastic-max} = -\frac{\Delta\varepsilon_{SH} \cdot E_C \cdot C_{3R}}{\frac{E_C}{E_S} C_{1R} + C_{2R}} \tag{13}$$

This enables the computation of the theoretical elastic stress as the sum of the incremented stress using incremental shrinkage, the elastic moduli of the concrete and steel, and the ring constants (C_{1R}, C_{2R}, and C_{3R}).

Fig. 7 illustrates the internal elastic pressure that would be expected for the rings using mixtures with material properties calculated using Eqs. (1) and (4). It should be noted that the thicker steel rings demonstrate a higher level of computed elastic stress since a higher level of restraint is provided by the thicker steel rings to resist the shrinkage of concrete.

In addition to computing the elastic stress, information from the approach outlined in this section can be used to determine the degree of restraint in the ring. Previous investigations have discussed the importance of the degree of restraint (ψ) on cracking potential [30–32]. Eq. (14) illustrates how the degree of restraint can be calculated using information from Eqs. (5) and (6).

$$\psi = \frac{U_{SH} - U_S|_{R_{OS}}}{U_{SH}} * 100\% \tag{14}$$

Fig. 8 illustrates the computed degree of restraint for the mixtures investigated in this study. First it can be clearly seen that thicker rings provide higher level of restraint

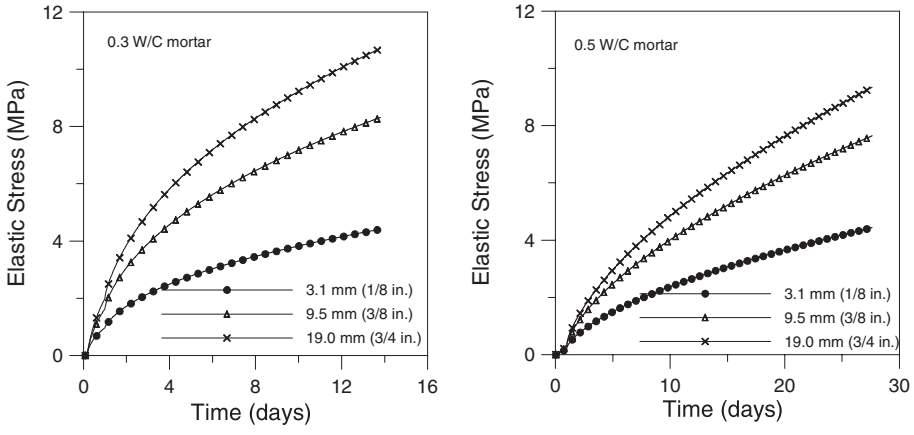

Fig. 7. Estimated elastic stresses in concrete ring specimens (with varying wall thickness).

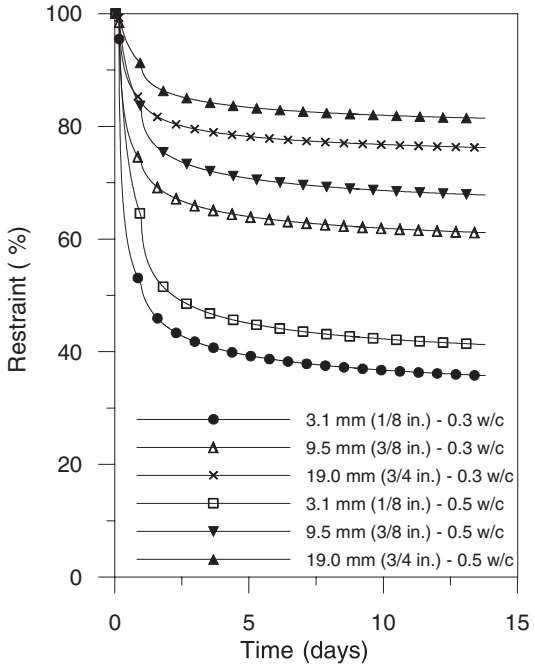

Fig. 8. Calculated degree of restraint.

than the thinner steel rings. Second, it can be seen that the degree of restraint varies with time due to the variation in elastic modulus of the concrete. In addition, comparison of the $w/c = 0.3$ and $w/c = 0.5$ mixtures shows that the degree of restraint is not constant for rings of similar dimensions as the shrinkage rate and elastic modulus of concrete influence the behavior. It can be seen that the degree of restraint varies by approximately 5–7% due to the difference in elastic moduli described in this paper.

3.2. Determination of actual residual stress

While the previous section provides a description of the stress that would be expected to develop if relaxation did not take place, this section will describe the actual residual stress that develops in concrete. To do this the ring can be separated into a concrete cylinder pressurized at the inner surface and steel cylinder pressurized with an equal and opposite pressure at the outer surface as shown in Fig. 9.

Dally and Riley [33] provide the solution for the radial displacement of a hollow cylinder (ring) exposed to uniform external pressure which can be used to describe the steel ring. Since the circumferential strain in the ring can be computed by dividing the radial displacement by the radius [16], the actual residual interface pressure (p_{Residual}) can be computed as the pressure required to cause a strain that is equivalent to the measured strain in the steel ($\varepsilon_{\text{Steel}}$) as shown in Eq. (15) [16,20].

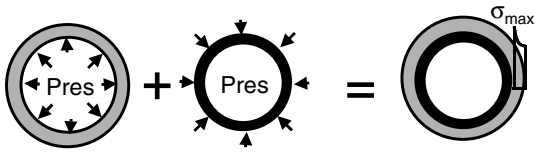

Fig. 9. Illustration of the idealization for computing the residual stress in the concrete.

$$p_{\text{Residual}}(t) = -\varepsilon_{\text{Steel}}(t)|_{r=R_{\text{IS}}} \cdot E_{\text{S}} \cdot \frac{\left(R_{\text{OS}}^2 - R_{\text{IS}}^2\right)}{2R_{\text{OS}}^2} \tag{15}$$

This illustrates that the actual residual interface pressure (p_{Residual}) can be determined using the steel properties, geometry of the steel ring, and average strain measured at the inner radius of the steel using the electrical resistance strain gages. This interface pressure can then be applied to the inside of the thick concrete ring and used to calculate the stresses in the concrete ring taking into account only the geometry of the concrete ring (i.e., no concrete properties are needed). Again, it can be shown that Eq. (15) can be greatly simplified by using a constant (C_{4R}) that depends only on wall thickness of the steel ring (assuming $v_{\text{S}} = 0.3$).

$$p_{\text{Residual}}(t) = -\varepsilon_{\text{Steel}}(t) \cdot E_{\text{S}} \cdot C_{4R} \tag{16a}$$

where C_{4R} is given as,

$$C_{4R} = \frac{R_{\text{OS}}^2 - R_{\text{IS}}^2}{2R_{\text{OS}}^2} \tag{16b}$$

The axi-symmetric nature of the problem eliminates the need to consider any circumferential tractions on the inner surface of the ring. The tensile stress (circumferential) at any point along the radial direction in the concrete ring can be related directly to the interface pressure (as shown previously in Eq. (11) using the actual residual pressure, p_{Residual}, in this case). Using the same simplifications shown in Eqs. (12b) and (16b) provides an expression for the actual circumferential maximum tensile stress that can be computed directly at any time, t, using Eq. (17):

$$\sigma_{\text{Actual-Max}} = -\varepsilon_{\text{Steel}}(t) \cdot E_{\text{S}} \cdot C_{3R} \cdot C_{4R} \tag{17}$$

Fig. 10 shows the actual maximum residual tensile stresses that were computed (using Eq. (17)) for the mixtures tested in this study. Several items of interest should be noted from these curves. First, the thicker steel rings demonstrate a higher stress level than thinner rings. This implies that the higher the degree of restraint, the higher the stress. It is interesting to observe that this difference in measured residual stress is very pronounced between the 3.1 mm (1/8 in.) and 9.5 mm (3/8 in.) wall thickness, yet much less noticeable for the thicker rings. The specimens with the thicker steel rings are observed to crack before the specimens cast around the thinner steel rings despite having similar average stress.

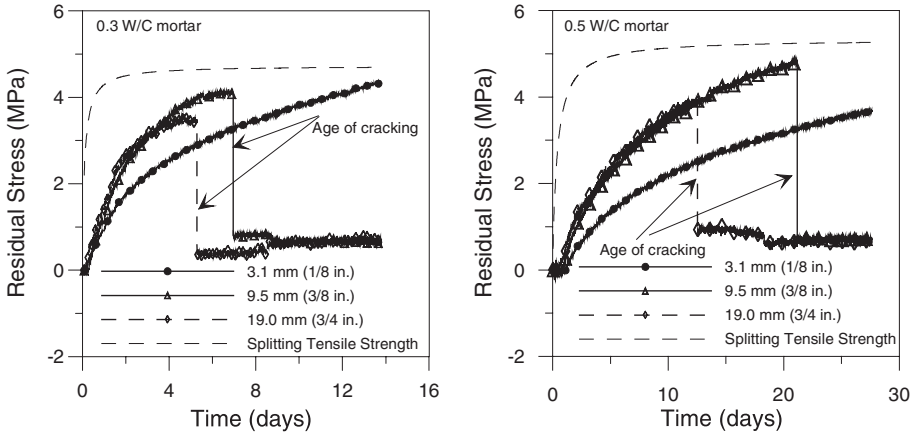

Fig. 10. Residual stress development in concrete ring specimens.

Although the reason for this is not completely understood, it is currently thought that this may be related to the development of damage (i.e. microcracking), however further investigation is needed to confirm this hypothesis.

3.3. Assessing the risk for cracking

The previous section described how the actual residual stress in the ring could be computed. By comparing this residual stress with the strength of a material provides a powerful tool to determine the cracking potential (Θ_{CR}) (i.e., the measure of how close the specimen may be to failure). The ability to determine the potential for cracking may be especially important in cases where cracking is not observed experimentally. While previous research has illustrated that a fracture mechanics approach may be preferred due to the size dependent tensile strength of a material [16], the cracking potential reported in this paper is based on the simple ratio of the actual residual stress and the splitting tensile stress as represented by Eq. (5).

$$\Theta_{CR} = \frac{\sigma_{Actual-Max}}{f_{sp}(t)} \tag{18}$$

Fig. 11 shows the computed values of the cracking potential for the mixtures tested in this investigation. While it is common to think that failure may be expected to occur when the cracking potential reaches 1, experimental evidence typically shows that cracking takes place at lower values [9]. It is interesting to note, however, that the value of the cracking potential does not appear to be consistent with varying levels of restraint.

3.4. Stress relaxation (creep effect)

The two stresses discussed in this paper (theoretical elastic and actual residual) can be used together to describe the effect of stress relaxation in restrained concrete. Fig. 12 illustrates one method that may be used to quantify the effect to relaxation by calculating the dif-

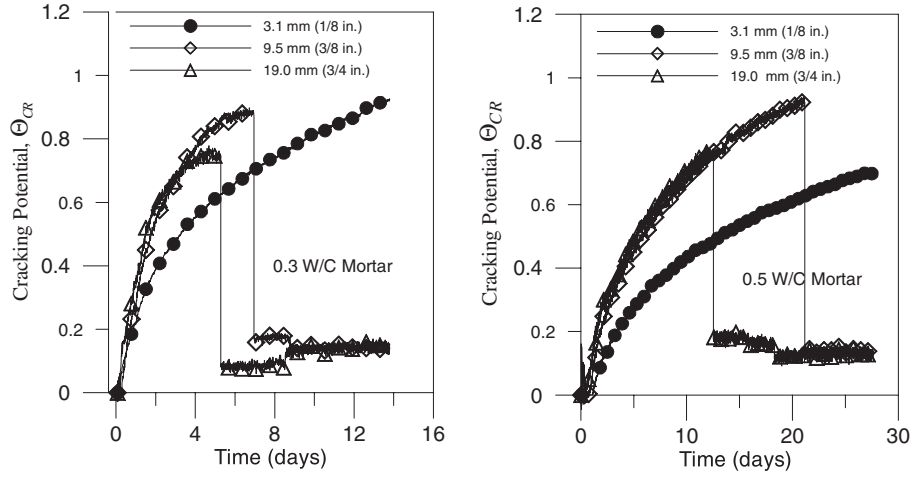

Fig. 11. Cracking potential of concrete ring specimens.

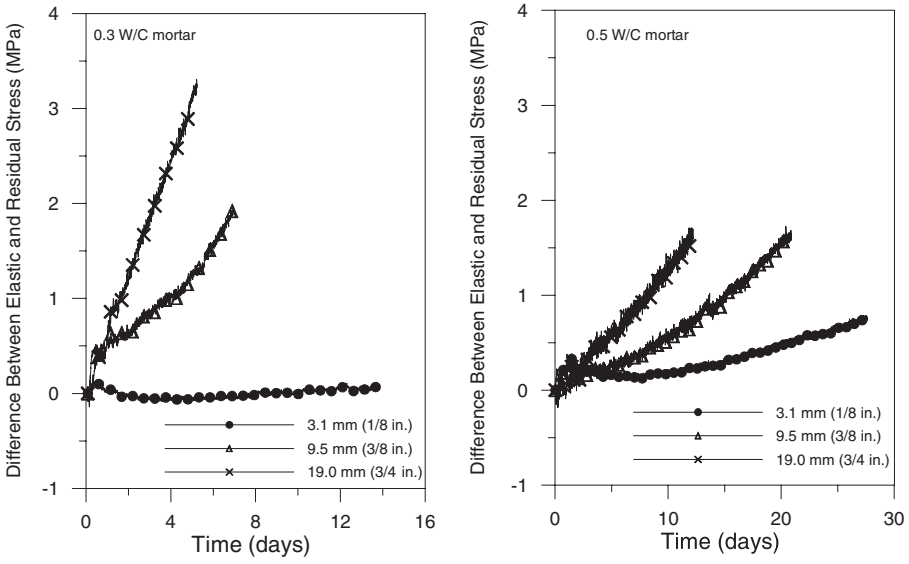

Fig. 12. Reduction in stress level due to creep relaxation in ring specimens.

ference between the theoretical elastic and actual residual stresses. Fig. 12 shows that the stress relaxation effect is more pronounced in the rings with a thicker steel wall. It is believed that this may be attributed to the fact that specimens with a thicker steel wall exhibit a higher degree of restraint, consequently the concrete in these rings can be thought of being tested under a higher load (i.e., a higher stress-to-strength ratio). Under these higher loads a greater potential for non-linear creep and microcracking would be expected. Since, the reduction in stress level due to creep is significant for the heavy steel rings, ignoring the effect of creep would introduce significant error in stress estimation. Although further work is needed to compare the ring measurements with more standard creep or relaxation measurements and to extend the data reduction to provide a more specific parameter such as specific creep or compliance, the approach shown in this paper provides an initial method which can be used to quantify the relaxation for a given specimen geometry.

4. Summary

This paper has demonstrated how the restrained ring test can be used to provide quantitative information on early-age stress development and early age cracking. The ring specimen allows tensile properties to be assessed without the difficulty of providing sufficient end restraint for tensile specimens. The ring specimen can be monitored immediately after the concrete is cast. Residual strain (stress) development was observed at very early-ages, corresponding roughly with the setting time of concrete. Equations are provided to calculate both the theoretical elastic stress in the ring (Eq. (13)) and the actual residual stress level that develops in the ring considering the effects of stress relaxation (Eq. (17)). Experiments conducted using steel rings of varying thickness indicated higher degree of restraint in the thicker rings which corresponded to a higher theoretical elastic stresses, greater stress relaxation, and earlier age of cracking. Analysis of the actual residual stress does not indicate a substantial difference between the stresses in the rings with a 9.5 mm (3/8 in.) or 19 mm (3/4 in.) wall suggesting potential for damage or non-linear creep effects, though further research is needed before a specific conclusion can be drawn. A ratio of the actual stress to strength is used to indicate how close a ring may be to failure even if cracking is not observed. It should be noted that the ratio of residual stress and strength does not appear to be constant at failure and increases with decreasing wall thickness and/or increased time to cracking. This suggests that a failure criterion based solely on strength may have potential to be improved. In conclusion, the approach presented in this paper provides an improvement to the existing qualitative ring test by allowing more quantitative information to be obtained from the tests, however further research is needed to relate this data to data obtained from other testing configurations.

Acknowledgements

The authors gratefully acknowledge support received from the Purdue Research Foundation and the Center for Advanced Cement-Based Materials (project C-1). This material is based upon work supported by the National Science Foundation under Grant No. 0134272: a CAREER AWARD granted to the second author.

This work was conducted in the Charles Pankow Concrete Materials Laboratory, as such the authors gratefully acknowledge the support which has made this laboratory and its operation possible.

References

[1] Bentur A. Chapter 6.5: Early-age cracking tests. RILEM state of the art report—early age cracking in cementitious systems, in Press.
[2] Weiss WJ, Yang W, Shah SP. Factors influencing durability and early-age cracking in high strength concrete structures, SP 189-22. In: High performance concrete: research to practice. Farmington Hills, MI: American Concrete Institute; 1999. p. 387–409.
[3] Grysbowski M, Shah SP. Shrinkage cracking of fiber reinforced concrete. ACI Mater J 1990;87(2):138–48.
[4] Weiss WJ, Yang W, Shah SP. Shrinkage cracking of restrained concrete slabs. ASCE Journal of Engineering Mechanics 1998;124(7):765–74.
[5] Springenschmidt R, Gierlinger E, Kernozycki W. Thermal stress in mass concrete: a new testing method and the influence of different cements. In: Proceedings of the 15th International Congress For Large Dams, Lausanne, R4, 1985. p. 57–72.
[6] Kovler K. Testing system for determining the mechanical behavior of early age concrete under restrained and free uniaxial shrinkage, RILEM, London, UK. Mater Struct 1994;27(170):324–30.
[7] Altoubat A, Lange DA. Creep, shrinkage, and cracking of early age concrete, ACI Mater J, accepted for publication.
[8] Toma G, Pigeon M, Marchand J, Bissonnette Bercelo L. Early-age autogenous restrained shrinkage: stress build up and relaxation, In: Persson B, Fagerlund G, editors. Self-desiccation and its importance in concrete technology, 1999. p. 61–72.
[9] van Breugel K, Lokhorst SJ. Stress-based crack criterion as a basis for the prevention of through cracks in concrete structures at early-ages. In: Kovler, K, Bentur, A., editors. RILEM International Conference on Early-Age Cracking in Cementitous Systems (EAC'01), Haifa Israel, RILEM, Paris, France. p. 145–58.
[10] Parilee AM, Buil M, Serrano JJ. Effect of fiber addition on the autogenous shrinkage of silica fume concrete. ACI Mater J 1989;86(2):139–44.
[11] Vepakomma S, Zollinger D, Jeong J-H. Characterization of cracking restraint at sawcut joints using the german cracking frame. In: 81st Annual Meeting of the Transportation Research Board, Washington DC, 2002.
[12] Altoubat SA, Lange D. Grip-specimen interaction in uniaxial restained test, ACI—special publication. Concrete: material science to application: a tribute to Surendra P. Shah, in press.
[13] Carlson RW, Reading TJ. Model of studying shrinkage cracking in concrete building walls. ACI Struct J 1988;85(4):395–404.
[14] Swamy RN, Stavarides H. Influence of fiber reinforcement on restrained shrinkage cracking. ACI J 1979;76(3):443–60.
[15] Kovler K, Sikuler J, Bentur A. Restrained shrinkage tests of fiber reinforced concrete ring specimens: effect of core thermal expansion. Mater Struct 1993;26:231–7.
[16] Weiss WJ, Yang W, Shah SP. Influence of specimen size and geometry on shrinkage cracking. J Eng Mech ASCE 2000;126(1):93–110.
[17] Attiogbe EK, See HT, Miltenberger MA. Tensile creeep in restrained shrinkage. In: Ulm FJ, Bazant ZP, Wittman FH, editors. Concreep 6: creep, shrinkage, and curability mechanic of concrete and other quasi-brittle materials, August 22–24. Cambridge MA: Elsevier; 2001. p. 651–6.
[18] Standard practice for estimating the crack tendency of concrete, AASHTO Designation PP-34-89, p. 179–82.
[19] NCHRP Report 380—Krauss PD, Rogalla EA, Sherman MR, McDonald DB, Osborn AEN, Pfeifer DW. Transverse Cracking in Newly Constructed Bridge Decks, NCHRP Project 12–37, 1995.
[20] Weiss WJ, Furgeson S. Restrained shrinkage testing: the impact of specimen geometry on quality control testing for material performance assessment. In: Ulm FJ, Bazant ZP, Wittman FH, editors. Concreep 6: Creep, Shrinkage, And Curability Mechanic of Concrete and Other Quasi-Brittle Materials, August 22–24. Cambridge, MA: Elsevier; 2001. p. 645–51.
[21] Barnes BD, Diamond S, Dolch WL. The contact zone between portland cement past and glass ''Aggregate'' surfaces. Cement Concrete Res 1978;8:233–44.
[22] ASTM. Concrete and aggregates. Annual book of ASTM standards 1994;Vol. 4.02.
[23] Tazawa E, editor. Japanese Concrete Institute Committee Report. Technical committee on autogenous shrinkage of concrete section 4 testing methods. Autoshrink 98, p. 55–65.
[24] Malhotra VM, Carino NJ, editors. CRC handbook on nondestructive testing of concrete. Florida: CRC Press; 1991. p. 101–46.
[25] Kayir H, Weiss WJ. Assessing the cracking caused by autogenous shrinkage in sealed low water-to-cement ratio systems, to be presented at the Annual Meeting of ACI, Phoenix, in preparation.
[26] Weiss WJ. Chapter 6.1: experimental determination of the 'time-zero' to (maturity-zero) MO. In: Bentur A., editor. Early age cracking in cementitious systems —state of the art report, 2002.
[27] Bazant ZP, editor. Fourth RILEM International Symposium on Creep and Shrinkage of Concrete: Mathematical Modeling, Northwestern University, 26–29 August, 1986.
[28] Graveen C. The use of non-destructive test methods to assess pavement quality in a performance-related specification, Purdue University, MS Thesis, W. Lafayette IN, May 2001.
[29] Timoshenko SP, Goodier JN. Theory of elasticity. McGraw-Hill Inc; 1987.
[30] Bissonnette B, Marchand J, Charron J, Delagrave A, Barcelo L. Early-age behavior of cement-based materials. In: Skalny J, Marchand J, editors. Material science of concrete VI. Westerville, Ohio: American Ceramic Society; 2000. p. 243–327.
[31] Shah SP, Weiss WJ, Yang W. Shrinkage cracking-can it be prevented? Concrete Int 1998;20(4):51–5.
[32] Bentur A, Berke NS, Dalliare MP, Durning T. Crack mitigation effects of shrinkage reducing admixtures ACI SP-204 In: Nawy FG, Frosch RJ, editors. Design and construction practices to mitigate cracking. USA: American Concrete Institute; 2001. p. 155–70.
[33] Dally JW, Riley WF. Experimental stress analysis. Third ed. McGraw-Hill, Inc; 1991.